INTERNATIONAL JOURNAL FOR NUMERICAL METHODS IN FLUIDS, VOL. 15, 1–22 (1992)

COMPUTER-AIDED DESIGN OF CHANNEL EXPANSIONS AND CONTRACTIONS

JOHANNES VASSILIOU SOULIS AND GEORGIA APOSTOLOU PSONI

Fluid Mechanics/Hydraulics Division, Civil Engineering Department, Democrition University of Thrace, Xanthi 67100, Greece

SUMMARY

A numerical method for designing open channel expansions and contractions to give a specified depth distribution is presented. The design of channels with prescribed depths–velocities is important because, amongst other things, boundary layer separation can be avoided. Cavitation can also be avoided by prescribing depth–velocity values that do not exceed certain critical values. The numerical scheme involves iteration between the direct solution (analysis) of a newly developed numerical algorithm and an inverse (design) solution. The governing system of PDEs is transformed into an equivalent system applied over a square grid network. The design procedure, which is based on two levels of design, yields a new set of co-ordinates for the channel geometry. This new geometry is used in the next iteration of the direct solution. Various channel expansions and contractions have been designed for supercritical flow conditions. Computed results also show how friction affects the channel shape. A numerical experiment has been carried out to establish the design capabilities. The new numerical procedure is a comparatively fast and reliable method for the purpose for which it was set forth. The method can be used either to generate entire new channel shapes or to modify regions of side walls.

KEY WORDS Hydraulic design Expansions–contractions Supercritical depth-averaged free surface flow Marching finite volume method

INTRODUCTION

In the motion of fluids in open channel configurations there are two general types of problems which must be answered. The first problem, which is the direct solution (analysis), requires the fluxes perpendicular to the side wall surfaces to be zero, while the velocities and flow depths of the flow field are the unknowns which have to be calculated. The second problem, which is the inverse solution (design), requires the Dirichlet boundary conditions to be applied, i.e. a flow distribution along the boundaries is specified and the shape of the boundaries must be determined.

Usually a design process involves the use of physical and/or numerical models to resolve the fluid properties adequately. Physical models considerably reproduce the details of the actual hydraulic structure but are usually subject to certain limitations of scale modelling. On the other hand, numerical models, which during the last 20 years have been dominating research methods, are also restricted to the validity of the governing equations representing the physical behaviour. However, the combined effects of the physical and numerical approaches can lead to significant designs acceptable from the engineering point of view. A computer-aided design will improve the performance of any hydraulic structure while at the same time shortening the amount of human effort needed for such a design. Until recently such designs were made iteratively by successive

0271–2091/92/130001–22$16.00

Received May 1991
Revised October 1991

modifications of the side wall geometries (cut and try) followed by direct (analysis) calculations. The design process was terminated soon after some acceptable results were derived. However, such a process is extremely time-consuming, resulting in considerably increased design costs. Alternatively, it is more efficient to use an inverse method, which, if it is directly linked with the direct solution, will make it possible to derive the proper side wall geometry from a flow depth distribution.

Expanding and contracting sections are usually utilized between channels of different cross-sectional areas in order to avoid undesirable flow conditions, e.g. cavitation, and to minimize head losses. Sometimes these sections are called transitions. Common types of transitions are inlet and outlet sections between canals and flumes, between canals and tunnels and between canals and inverted siphons.[1] In a transition there is nearly always appreciable change in the flow depth with subsequent alterations in flow velocities. Whenever supercritical flows are occurring, a change in alignment of the transition walls creates standing wave patterns, overtopping, excessive structural loading and non-uniform flow in the downstream region. However, slight alterations in curvature of the side walls constitute a delicate problem which needs special attention.

One of the most common causes of spillway failures has been the improper design of steep chutes. In chute design it is usually required to determine the dimensions that will provide for a given discharge. The requirements for the correct shaping of the chute side walls are often overlooked. Whenever the crest length of a spillway is greater than the width of the energy dissipator, the chute must converge in the downstream direction.[2] However, the flow in a chute is always supercritical and the design of the shape in plan of the chute side walls is a very difficult problem.

Also, channel expansion in supercritical flows occurs frequently at places where flow emerges at high speed, e.g. from a closed conduit or a sluice gate. A satisfactory design for the expansion is of practical importance, since if an expansion is designed to diverge too rapidly, the flow will fail to follow the boundaries; on the other hand, if the expansion is too gradual, waste of materials will result and finally, if the local disturbances produced by improper boundary geometry are of great height, the walls will fail to confine the flow.

While it is true that nearly all analysis codes can be converted into design codes, from a general literature survey it is apparent that design procedures for two-dimensional free surface flow hydraulic structures are virtually non-existent. Most of the experience of design codes comes straight from compressible flow theories. Therefore, to demonstrate the experience to date, a quick literature survey is made on numerical designs dealing with compressible flows. Singh[3] derived a time-marching method which generates blade profiles in a cascade corresponding to a prescribed pressure distribution around blade surfaces. Tranen[4] produced a numerical method for the design of two-dimensional aerofoil sections with a prescribed transonic pressure distribution. Soulis[5] presented a numerical method for the design of thin turbomachinery blades with specified whirl velocities across the blade span. The method was used to design free vortex thin blades for turbines and compressors operating in incompressible and compressible (subsonic) flow regimes using the potential function concept. Stanitz[6] designed two-dimensional channels with a specified velocity distribution along the channel walls for both incompressible and compressible flows. Brown and Eskandarian[7] derived a method for propulsion nozzle design based on Tranen's method. A mass flux balance was written to calculate the displacements of the streamlines across the nozzle solid bodies. A similar approach is applied by Hart and Whitehead[8] in order to design two-dimensional cascades of turbomachinery blades based on finite element analysis. Tong and Thomkins[9] have presented a finite volume approach for the design of shock-free or strong passage shock turbomachinery cascades. Finally, Borges[10] presented

a three-dimensional approach for the design of an impeller of a low-speed radial inflow turbine. His approach is similar to that reported by Soulis.[5]

Rouse *et al.*,[11] as early as the late 1940s, obtained practical results which were found useful in the preliminary design of channel expansions in supercritical flow. Their results refer to abrupt expansions, efficient gradual expansions and generalized boundary curves for channel expansions. Ippen[12] describes the mechanics of supercritical flow for converging boundaries. His basic formulation and design procedures have been incorporated into a computer spillway design procedure by Traubert.[13] Knapp,[14] in order to eliminate or reduce superelevation and crosswave disturbance patterns in curved channels, suggested various simple design methods for banking, multiple curved vanes, easement curves and diagonal sills. Finally, Bauer and Beck[15] describe simple rules for the design of side walls in spillway chutes.

A two-dimensional design method with prescribed flow depths–velocities along the side walls is presented. The numerical scheme involves iteration between the direct solution of a newly developed numerical algorithm[16] and an inverse solution. The analysis code solves the governing equations on a non-orthogonal co-ordinate system. Therefore irregular flow regions can be analysed easily and efficiently. All applications refer to supercritical flow conditions through the flow field. The method reported herein was developed in our Computation Laboratory during 1990. The method was coded in FORTRAN and run on a MicroVax II as well as on a VAX 8350 computer.

ANALYSIS

Flow equations

Under the assumption of homogeneous, incompressible, two-dimensional, viscous flow with hydrostatic pressure distribution, the governing free surface flow equations for the physical domain in the Cartesian co-ordinate system are

$$\mathbf{W}_t + \mathbf{F}_x + \mathbf{G}_y = \mathbf{D}, \tag{1}$$

where

$$\mathbf{W} = \begin{bmatrix} h \\ hu \\ hv \end{bmatrix}, \qquad \mathbf{F} = \begin{bmatrix} hu \\ hu^2 + gh^2/2 \\ huv \end{bmatrix}, \tag{2}$$

$$\mathbf{G} = \begin{bmatrix} hv \\ huv \\ hv^2 + gh^2/2 \end{bmatrix}, \qquad \mathbf{D} = \begin{bmatrix} 0 \\ gh(S_{0x} - S_{fx}) \\ gh(S_{0y} - S_{fy}) \end{bmatrix}. \tag{3}$$

The system of equations (1) is of the conservative form capable also of dealing with hydraulic jumps. In the above system h is the water depth, u and v are the velocity components along the axial (x) and tangential (y) flow directions respectively, g is the acceleration due to gravity, S_{0x} and S_{0y} are the channel slopes in the x- and y-direction respectively and S_{fx} and S_{fy} are the respective friction slopes, which are defined as

$$S_{fx} = \frac{n^2 u\sqrt{(u^2+v^2)}}{h^{4/3}}, \qquad S_{fy} = \frac{n^2 v\sqrt{(u^2+v^2)}}{h^{4/3}}, \tag{4}$$

where n is the Manning flow friction coefficient.

The essence of the proposed scheme is that quadrilaterals in the physical domain will be separately mapped into squares in the computational domain by independent transformations

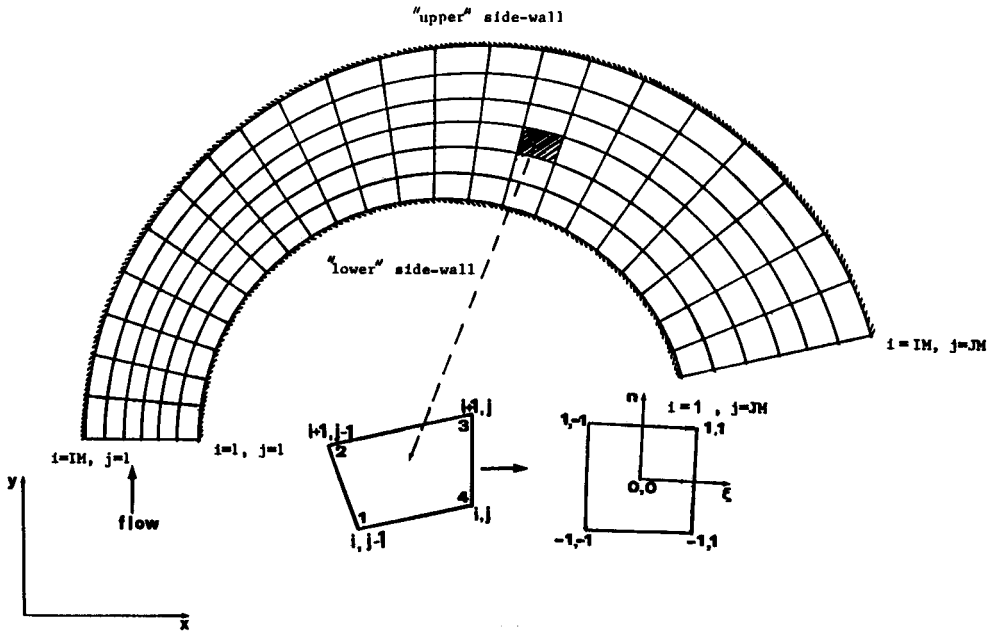

Figure 1. Sparse computational grid and mapping

from Cartesian (x, y) to local (ξ, η) co-ordinates as illustrated in Figure 1. If x_i and y_i are the Cartesian co-ordinates of the corners of a finite volume, then the co-ordinates of any point of this finite volume can be expressed as

$$x=\sum_1^4 N_i x_i, \qquad y=\sum_1^4 N_i y_i, \tag{5}$$

where N_i are the shape functions associated with the finite volume nodes. The shape functions are defined in terms of a local non-orthogonal co-ordinate system (ξ, η) as

$$N_1=(1-\xi)(1-\eta)/4, \qquad N_2=(1+\xi)(1-\eta)/4, \qquad N_3=(1+\xi)(1+\eta)/4, \qquad N_4=(1-\xi)(1+\eta)/4. \tag{6}$$

Let $\mathbf{J}^{-1}$ be the transformation matrix from the physical to the computational local co-ordinate system:

$$\mathbf{J}^{-1}=\begin{bmatrix} x_\xi & x_\eta \\ y_\xi & y_\eta \end{bmatrix}. \tag{7}$$

The following relations hold:[16]

$$\mathbf{W}'_t+\mathbf{F}'_\xi+\mathbf{G}'_\eta=\mathbf{D}', \tag{8}$$

where

$$\mathbf{W}'=J^{-1}\begin{bmatrix} h \\ hu \\ hv \end{bmatrix}, \qquad \mathbf{F}'=J^{-1}\begin{bmatrix} hU \\ hUu+\xi_x gh^2/2 \\ hUv+\xi_y gh^2/2 \end{bmatrix}, \tag{9}$$

$$\mathbf{G}' = J^{-1}\begin{bmatrix} hV \\ hVu+\eta_x gh^2/2 \\ hVv+\eta_y gh^2/2 \end{bmatrix}, \quad \mathbf{D}' = J^{-1}\begin{bmatrix} 0 \\ gh(S_{0x}-S_{fx}) \\ gh(S_{0y}-S_{fy}) \end{bmatrix}. \tag{10}$$

J^{-1} is the determinant of the matrix $\mathbf{J}^{-1}$, U and V are the velocity components in the computational domain, while the velocity components u and v in the physical domain are

$$\begin{bmatrix} u \\ v \end{bmatrix} = J^{-1}\begin{bmatrix} U \\ V \end{bmatrix} \tag{11}$$

Also,

$$x_\xi = J^{-1}\eta_y, \qquad x_\eta = -J^{+1}\xi_y, \qquad y_\xi = -J^{-1}\eta_x, \qquad y_\eta = J^{-1}\xi_x. \tag{12}$$

Boundary conditions

At the upstream boundary the transverse flow direction component of velocity is specified. A uniform (across the width) flow depth is also specified along with the total available head. At the downstream end no boundary conditions are required to be enforced. All the above conditions are applicable to supercritical flow throughout the field. When the condition of no flow across the side walls is applied, the mass fluxes are taken across the faces of the boundary finite volume which is bounded on one face by the solid body. Thereafter the flux components hu and hv for the side wall surfaces are recalculated requiring the component of velocity normal to the solid surfaces, q_n, to be zero.

Numerical procedure

The two-dimensional flow equations (8) may be written as conservation form equations for a control volume ΔV of unit height and for a time step Δt as

$$-\Delta(J^{-1}h) = [\Delta(J^{-1}hU)\Delta\eta + \Delta(J^{-1}hV)\Delta\xi]\Delta t/\Delta\xi\Delta\eta \quad \text{(continuity)}, \tag{13}$$

$$-\Delta(J^{-1}hu) = \{\Delta[J^{-1}(hUu+\xi_x gh^2/2)]\Delta\eta + \Delta[J^{-1}(hVu+\eta_x gh^2/2)]\Delta\xi\} \times \Delta t/\Delta\xi\Delta\eta - J^{-1}gh(S_{0x}-S_{fx})\Delta t \quad (\xi\text{-momentum}), \tag{14}$$

$$-\Delta(J^{-1}hv) = \{\Delta[J^{-1}(hUv+\xi_y gh^2/2)]\Delta\eta + \Delta[J^{-1}(hVv+\eta_y gh^2/2)]\Delta\xi\} \times \Delta t/\Delta\xi\Delta\eta - J^{-1}gh(S_{0y}-S_{fy})\Delta t \quad (\eta\text{-momentum}). \tag{15}$$

Thus for the *mass flux* an XFLUX at i,j is defined as

$$(\text{XFLUX})_{i,j} = [(J^{-1}hU)_{i,j} + (J^{-1}hU)_{i+1,j}]\Delta\eta/2, \tag{16}$$

while the YFLUX at the same point is defined as

$$(\text{YFLUX})_{i,j} = [(J^{-1}hV)_{i,j} + (J^{-1}hV)_{i,j-1}]\Delta\xi/2. \tag{17}$$

The terms $\Delta(J^{-1}hU)$ and $\Delta(J^{-1}hV)$ in equation (13) are defined as

$$\Delta(J^{-1}hU) = (\text{XFLUX})_{i,j} - (\text{XFLUX})_{i,j-1}, \tag{18}$$

$$\Delta(J^{-1}hV) = (\text{YFLUX})_{i+1,j} - (\text{YFLUX})_{i,j}. \tag{19}$$

Similar differencing is adopted for the *ξ-momentum* and *η-momentum flux balances*, equations (14) and (15) respectively. The governing flow equations are solved in the order: continuity, η-momentum, ξ-momentum. The bottom slopes S_{0x} and S_{0y} are precalculated and stored, while the

friction slopes S_{fx} and S_{fy} are updated at each time step. The changes $\Delta(J^{-1}h)$, $\Delta(J^{-1}hu)$ and $\Delta(J^{-1}hv)$ of the LHS of equations (13)–(15) respectively are used to estimate the new values for h, u and v. Thereafter a new iteration step is performed.

DESIGN

Boundary conditions

When initiating the design process, a starting geometry must be residing in core (see Figure 2). It is usual practice to estimate the initiating side wall geometry as closely as possible to the expected one. However, this is not always possible and therefore an arbitrary shape is defined.

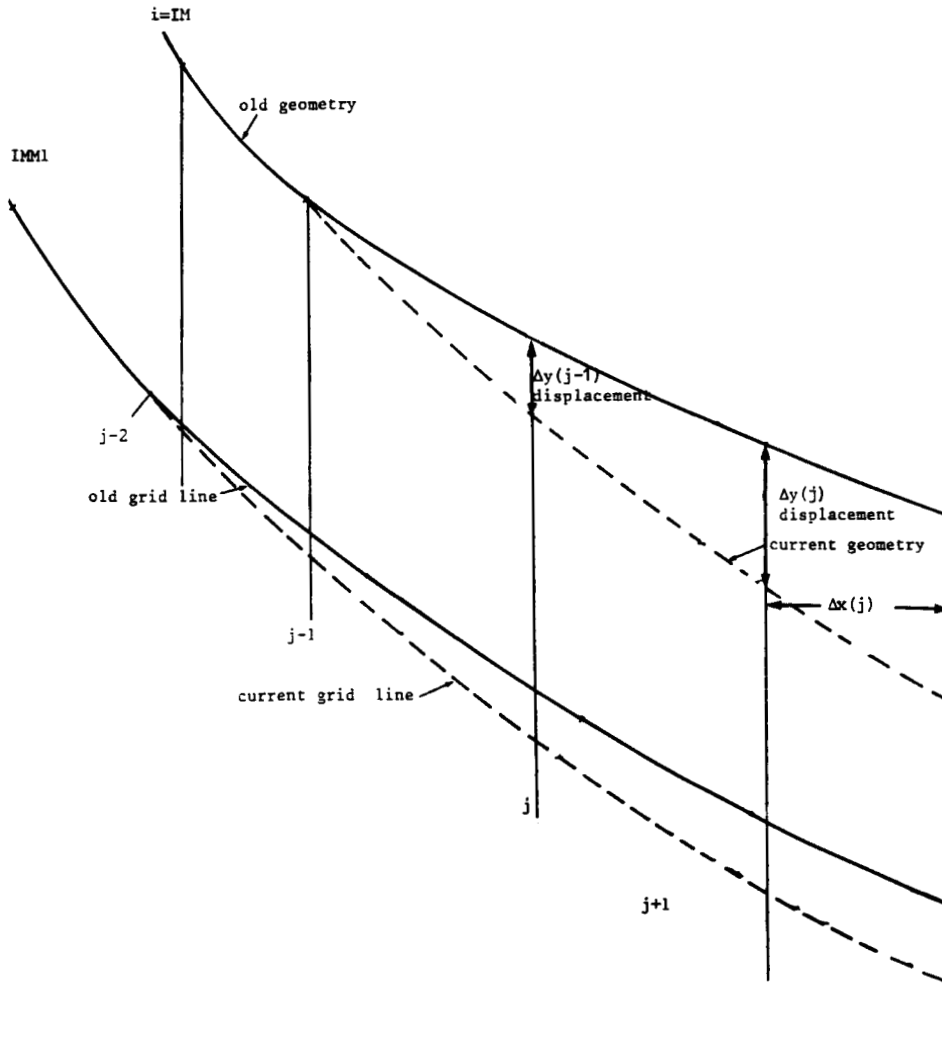

Figure 2. Notation for wall displacements

This geometry is usually relaxed before it is incorporated into the design procedure. A properly guessed initial geometry will decrease the amount of CPU time needed for design and at the same time will certainly avoid failure in the numerical procedure. It is also necessary to specify as data the inlet and outlet widths of the structure under design. These widths remain fixed throughout the course of the iterations. The inlet angle of the side walls under formation remains fixed. The outlet angle of the structure is initially given a value in order to start the iterations. This angle is permitted to change. The design procedure needs the distributions of S_{0x} and S_{0y} throughout the computational field. The Manning flow friction coefficient n is also specified. Finally, the axial positions of the inlet and outlet ends are held fixed; thus the axial distance between the inlet and outlet is fixed. Of course, the real lengths of the side walls change as the modified geometry tends to satisfy (through the calculated flow field) the required flow depth distribution. Table I shows the solid boundary conditions used in the design.

At a given inlet total available head H_{01}, water flow depth h_1 and velocity component v_1 a desired water flow depth distribution along the channel side walls is prescribed. Thus the flow discharge through the hydraulic structure is determined. In the current method a prescribed value of depth, h_{pre}, is allocated at each grid point of the 'upper' ($i=IM; j=1, JM$) and 'lower' ($i=1; j=1, JM$) mobile side walls of the flume (see Figure 3). With minor computing code modifications it is possible to prescribe many possible depths along the axial distance of the hydraulic structure under design, which in turn satisfy particular design needs. The outlet flow region remains totally free from any conditions. Emphasis must be put on the fact that all the above flow conditions as well as the associated design procedures are primarily intended for supercritical flow conditions. Table II shows the fluid boundary conditions used in the design.

Table I. Solid boundary conditions needed for design

Geometry condition	Fixed	Allowed to change
S_{0x}	√	
S_{0y}	√	
n (Manning)	√	
Inlet width	√	
Outlet width	√	
Inlet position x, y	√	
Outlet position x	√	
Outlet position y		√
Inlet angle	√	
Outlet angle		√
Initial geometry		√
Side wall geometry		√
Computational grid		√
Axial grid locations	√	

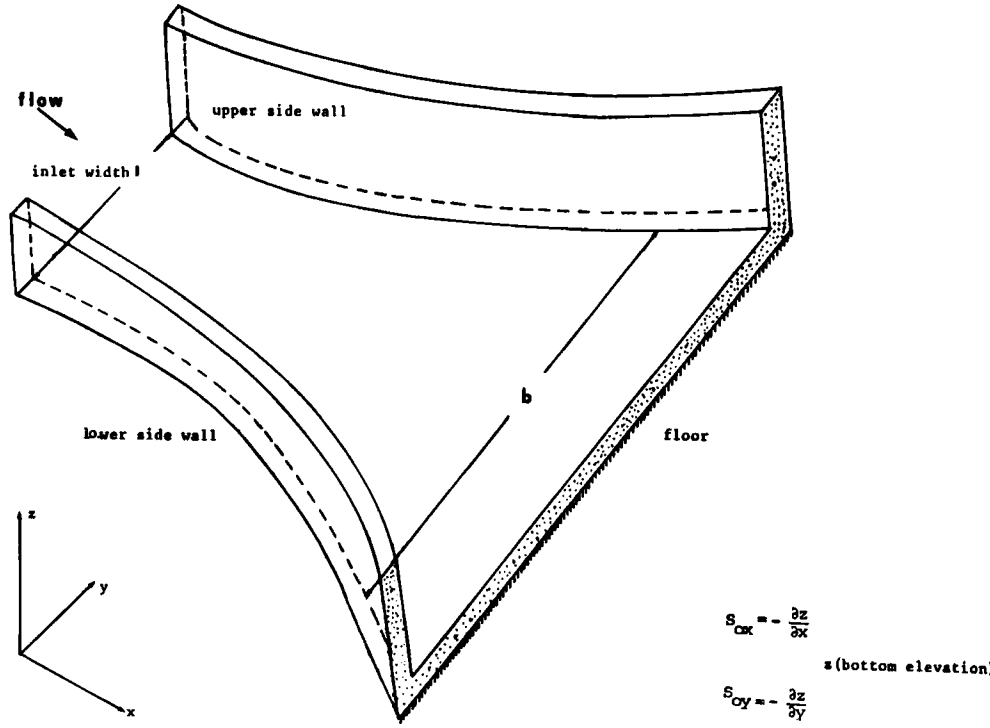

Figure 3. Definition of a typical channel expansion geometry

Table II. Fluid boundary conditions needed for design

Flow condition	Fixed	Allowed to change
H_{01}	√	
h_1	√	
v_1	√	
$h_{pre}(i=1; j=1, JM)$	√	
$h_{pre}(i=IM; j=1, JM)$	√	
$q_{pre}(i=1; j=1, JM)$	√	
$q_{pre}(i=IM; j=1, JM)$	√	
$h(i=2, IMM1; \quad j=2, JM)$		√
$u(i=1, IM; \quad j=2, JM)$		√
$v(i=1, IM; \quad j=2, JM)$		√
S_{fx}		√
S_{fy}		√

Determining the new channel geometry

In the analysis the concept of tangential velocity along the walls is enforced. In the design stage, to provide the Dirichlet boundary condition, the prescribed flow depth distribution is enforced. In the current research work this is a twofold numerical procedure.

In the *first scale*, on the mobile boundaries, new streamline positions are found from the flow angle θ. This flow angle is calculated from the equation

$$\tan\theta = u/v, \tag{20}$$

where u and v are the current iteration step velocities along the 'upper' and 'lower' surfaces respectively. The calculation starts at the inlet position and is based on the fact that the axial differencing $\Delta x(j)$ is held constant (see Figure 2 as well as Table I). The displacements $\Delta y(j)$ are calculated from

$$\Delta y(j) = \Delta x(j) \tan\theta \tag{21}$$

for each θ. These displacements are added to the old ys of either mobile wall in order to yield the new ys. The current version of the computational grid utilizes grid lines perpendicular to the axial direction. Thus at each grid point of the side walls (see Figure 2) new positions are calculated. However, this procedure is only applied after a certain number of iterations, usually 40 or so, whenever there is sufficient indication of convergence of the analysis code. Numerical experimentation has shown that sufficient convergence means that the percentage average (over the flow field) change in the axial velocity u from the previous iteration is less than 0·001%. At the same time the maximum and average values of shifts of the mobile boundaries are calculated. If these values are higher than 0·005% (maximum) or 0·0001% (average) of the outlet width, then the analysis is repeated again and again until the values become lower than 0·005% and 0·0001%.

The *second scale* is initiated soon after the previously mentioned criterion is satisfied. As the solution converges, the shift of the streamlines becomes negligible. The iterations are repeated and the resulting flow depths are compared with the prescribed h_{pre} set forth initially. If the maximum

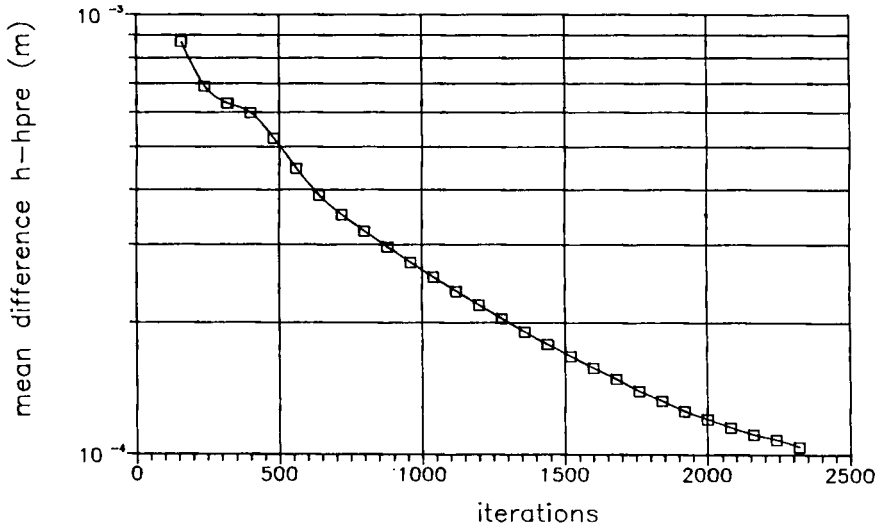

Figure 4. Convergence history of Design 2

difference between these values is higher than 0·001% of the inlet total head H_{01} or if the average difference between these values is higher than 0·0001% of H_{01}, then a new local tangential displacement (DISPL) of the mobile side walls is calculated[3] according to

$$\text{DISPL} = \frac{(\Delta x^2 + \Delta y^2)^2}{\Delta x^2 l \text{ALEF}} \frac{q - q_{\text{pre}}}{q}, \tag{22}$$

where l is the inlet width (see Figure 3), ALEF is a factor which usually takes values between 0·1 and 1·0, q is the current value of the velocity $\sqrt{(u^2+v^2)}$ and q_{pre} is the prescribed velocity along the mobile walls. The value of q_{pre} is calculated from the total available head as well as from the flow depths at each grid point. This calculation is performed using Bernoulli's equation. Two versions of this equation are applied. The first version refers to ideal flow while the second one refers to inclined flow with friction. As the solution converges, the differences $q - q_{\text{pre}}$ become negligible and subsequently the calculated displacement also becomes negligible. If the second criterion is satisfied, i.e. if the maximum or average difference between h and h_{pre} becomes less than 0·001% or 0·0001% respectively of H_{01}, the design procedure is terminated. The utilization of two convergence criteria was found to be necessary in order to eliminate local error instability. Figure 4 shows the mean (along the mobile walls) $h - h_{\text{pre}}$ variation with the number of iterations for a typical application (Design 2).

Computation

The flowchart of the computational scheme is given in Table III.

After a specified number of iterations of the direct solution, subsequently called NDS, the numerical scheme incorporates the design procedure. This number depends on (a) the type of supercritical flow, (b) the geometrical complexity of the initial configuration and (c) the finally sought geometry. This number is typically 40 or so iterations, when there is sufficient indication that the change in the flow properties from the previous iteration values is small. Figure 5 shows the effects of this number on the total number of iterations required for Design 2. Values of NDS higher than 40 delay the convergence rate for nearly all application examples. On the other hand, values of NDS less than 40 prevent the settling down of the flow field before the incorporation of the design process. As a result the numerical solution breaks down. Numerical experimentation

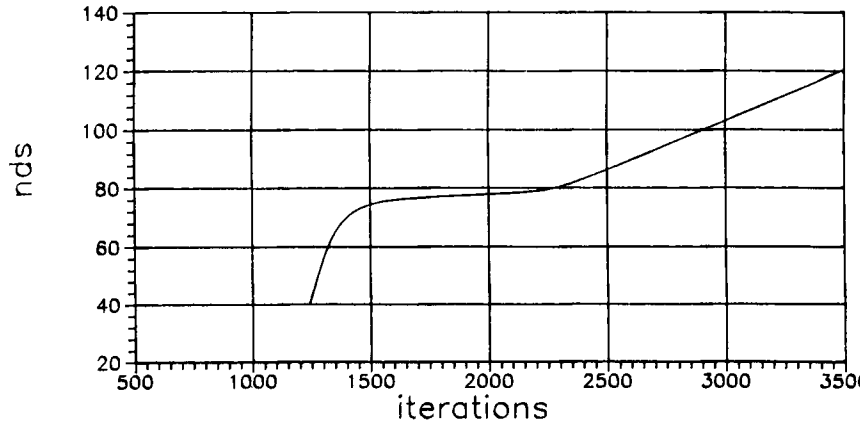

Figure 5. The choice of NDS (number of direct solutions) affects the convergence solution (Design 2)

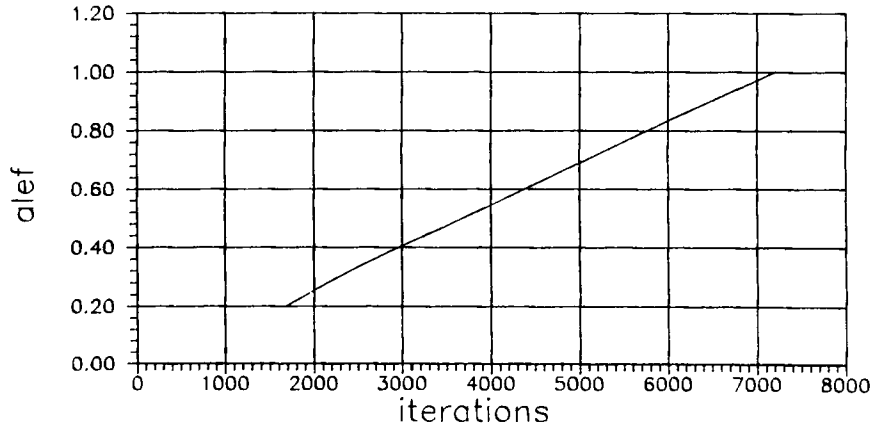

Figure 6. The ALEF factor of equation (22) can accelerate the convergence solution

has shown that in order to achieve convergence, the design procedure needs to be incorporated 15–30 times. When the initial geometry yields flow depth distributions with considerable differences from the prescribed values, it is found to be necessary to relax the currently estimated geometry before it is used in the iteration of the direct solution:

$$y_{i,j}^{n+1} = \omega \tilde{y}_{i,j} + (1-\omega) y_{i,j}^{n+1}, \quad i=1, IM; \quad j=1, JM; \tag{23}$$

where the overtilde denotes the current value and ω is a relaxation factor. Thereafter the new computational grid is formed. New Jacobians and partial derivatives x_ξ, x_η, y_ξ and y_η must be calculated for each finite volume of the new flow field.

As the solution advances, new flow directions are calculated for the mobile walls. The new wall positions are considered to be streamline-like. Of course, in the new position some mass flow is crossing through the mobile walls. This is due to the fact that the solution has not yet fully converged. However, as the solution proceeds, this mass flux becomes small. Eventually, the new geometry freezes and therefore a test is needed to ensure that the design target has been fulfilled. The previously mentioned design criteria are initiated through the subroutines DES1 and DES2 (see Table III). At the very end the differences between q and q_{pre} become negligible and the whole solution procedure yields a frozen geometry, the one sought. The effect of the ALEF factor (equation (22)) on the local displacement and eventually on the convergence rate for a typical application (Design 2) is shown Figure 6. A lower limit of ALEF exists, 0·20, below which the numerical solution breaks down. A typical computational grid is formed by 16×50 (transverse $\times$ axial) points. Denser computational grids did not essentially change the computed results. For a typical design the amount of required CPU time on a MicroVax II computer was 1380 s. Several test cases were carried out on a PC. For the majority of the presented design examples the method proved to be reliable and fast. The proper selection of ω, ALEF and l accelerates the solution convergence rate provided that extreme values are avoided.

DESIGN EXAMPLES

In order to validate the design calculations, it was desirable to know in advance what geometry each of the prescribed flow depths corresponds to under specified inlet flow conditions. Thus it would have been immediately apparent whether or not the design procedure resulted in the

Table III. Flowchart for design process

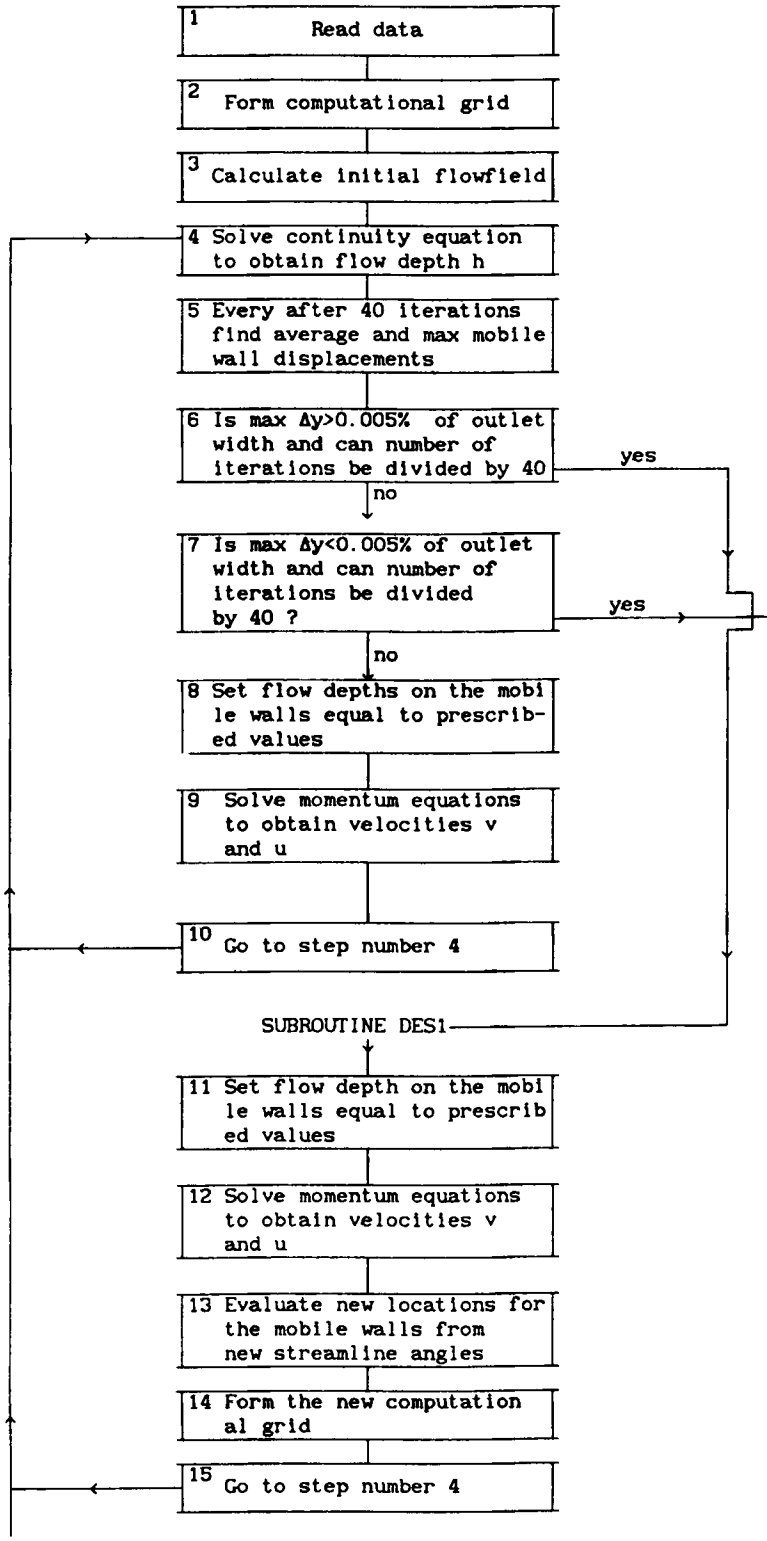

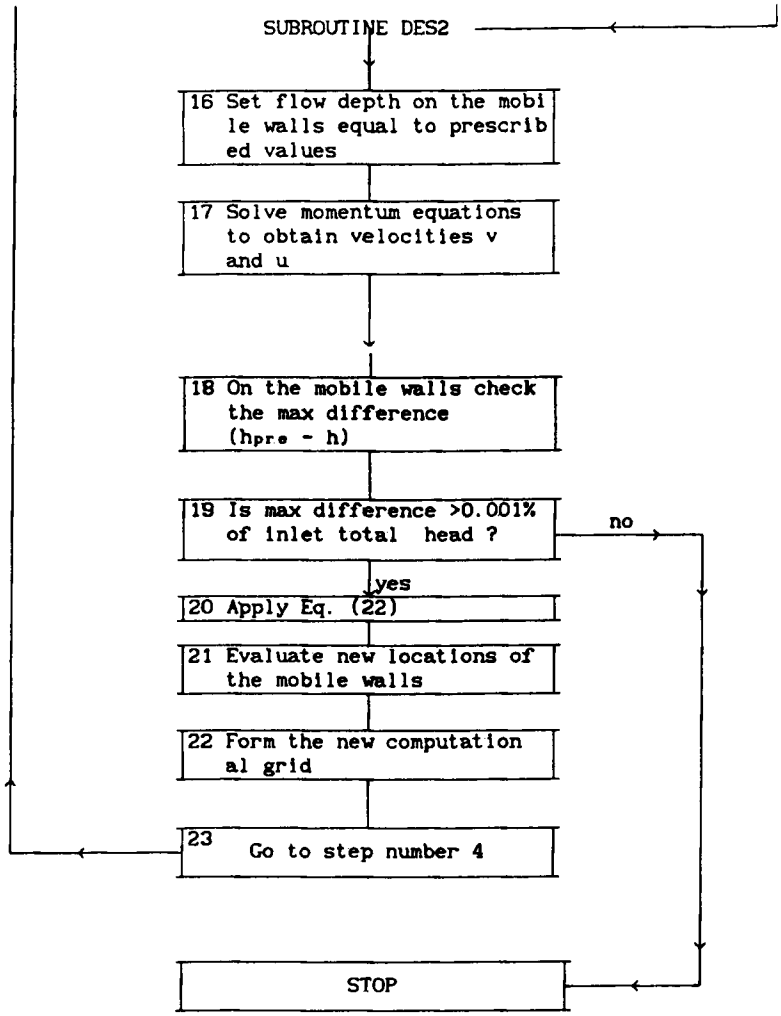

desired channel geometry. In fact, the computer code development was done against a simple expansion design (Design 2) where the side walls comprised straight surfaces. Emphasis must be put on the fact that for all tested designs the cross-section is rectangular. Thus any programming error would have been easily identified since either the solution would diverge or it would have ended up in a wrong design. Table IV shows the geometrical–physical conditions and the results of the applied test cases in which flow friction is present.

Inlet transition design (Design 1)

In the first test case it was required to design a symmetrical inlet structure connecting a canal to a flume. The hydraulic properties are given in Table IV. The initial geometry is shown in Figure 7, while the desired and derived flow depths are shown in Figure 8. Hinds[17] presented a simple numerical procedure for one-dimensional transition designs. The calculated results using the method of Hinds are compared with the current method results in Figure 7. Some differences are

Table IV. Geometrical–physical conditions and results of design examples

Flow/geometry	Design 1 Inlet transition	Design 2 Straight line	Design 3 Rouse *et al.*[11] $Fr_1=2{\cdot}0$	Design 4 Rouse *et al.*[11] $Fr_1=4{\cdot}0$	Design 5 Constant flow depth
H_{01} (m)	4·52	5·25	3·0	9·0	1.8
h_1 (m)	1·40	1·75	1·0	1·0	0·6
Fr_1	2·11	2·0	2·0	4·0	2·0
v_1 (m s^{-1})	0·0	0·0	0·0	0·0	0·0
S_{0x}	0·0	0·05	0·0	0·0	0·05
S_{0y}	0·0	0·0	0·0	0·0	0·0
n	0·012	0·012	0·012	0·012	0·012
Initial geometry	Figure 7	Figure 9	Figure 11	Figure 13	Figure 15
Prescribed flow depths	Figure 8	Figures 10(a, b)	Figures 12(a, b)	Figures 14(a, b)	Figure 16
Designed geometry	Figure 7	Figure 9	Figure 11	Figure 13	Figure 15
Derived flow depths	Figure 8	Figures 10(a, b)	Figures 12(a, b)	Figures 14(a, b)	Figure 16

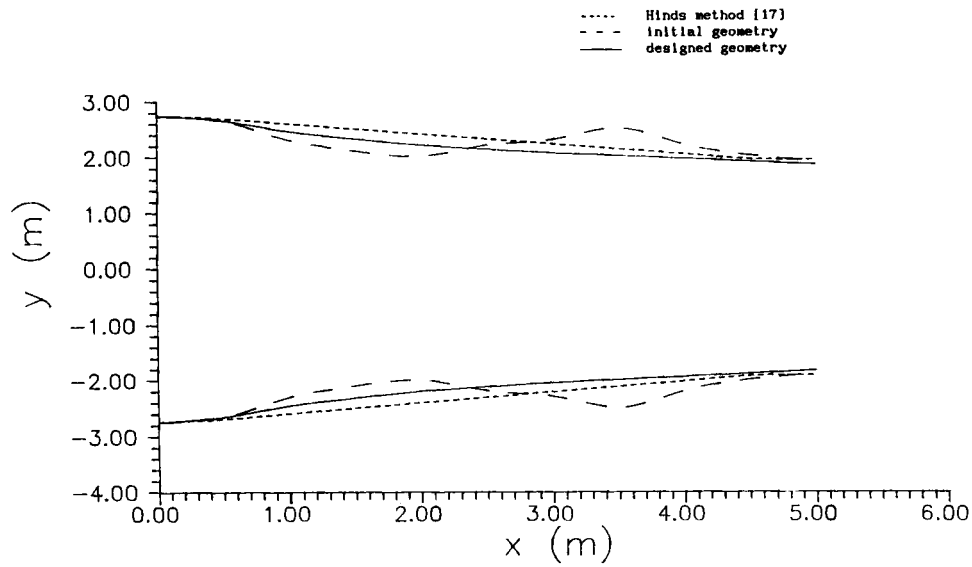

Figure 7. Comparison between present and Hinds'[17] (1D) method designed inlet transition geometry at $Fr_1 = 2{\cdot}11$. The figure also shows the initial geometry of the current method

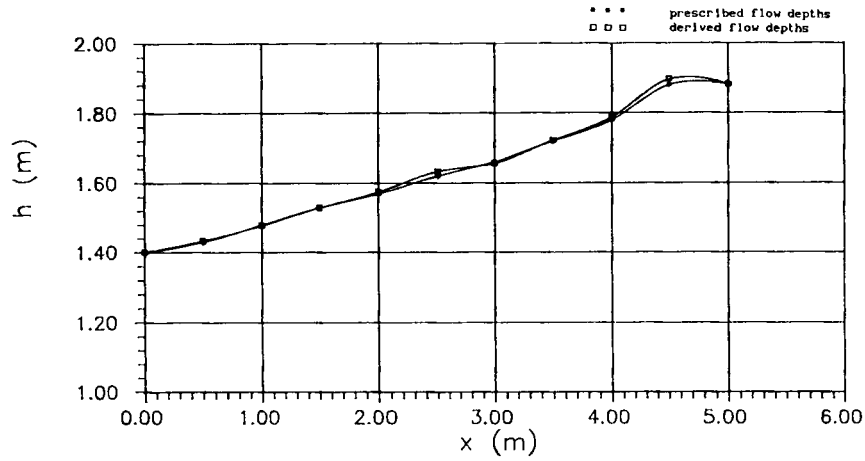

Figure 8. The direct solution using the designed geometry of Figure 7 compared with the prescribed flow depths

apparent. It is believed that these differences are due to the fact that Hinds' method is a one-dimensional approach while the test case under design is clearly a two-dimensional problem. The comparison also serves as a guideline for estimating the errors between one- and two-dimensional design approaches.

Straight line expansion design (Design 2)

The second test case was a straight line expansion design at an inlet Froude number of 2·0. It is on this design that the computing code development was mainly done. It was decided to deform

only the 'upper' side wall. The other one remained identical to the finally sought solution. However, the deformation from the correct solution was made severe in order to test the computing code capabilities. The initial geometry of the expansion is shown in Figure 9. The desired water depth distributions along the 'lower' and 'upper' side walls are shown in Figures 10(a) and 10(b) respectively. The designed geometry is shown in Figure 9. Some convergence

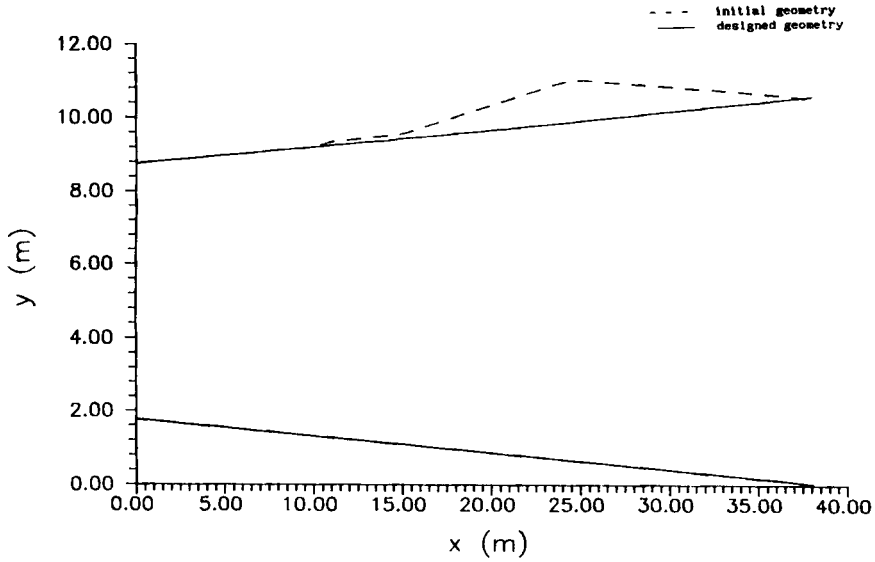

Figure 9. Initial and designed geometries for the straight line expansion design example at $Fr_1 = 2{\cdot}0$

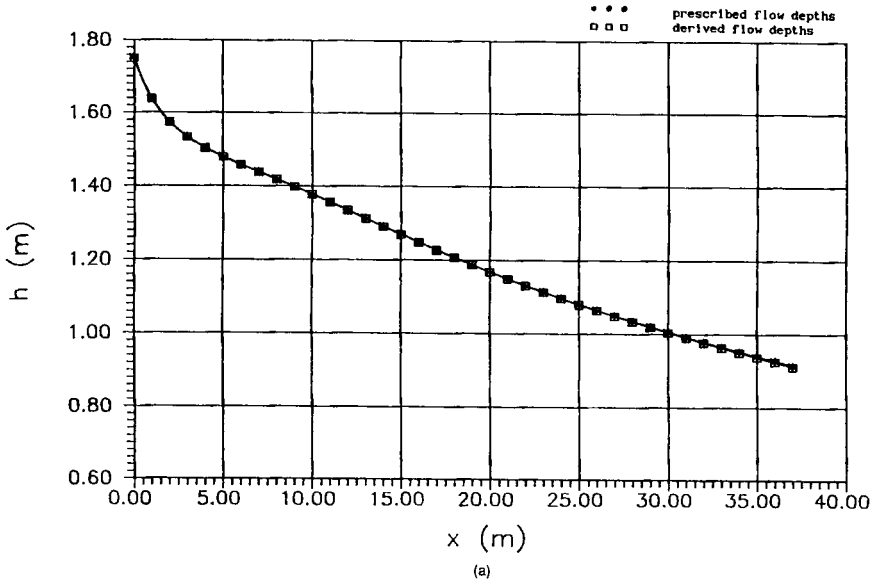

Figure 10(a). The direct solution using the designed geometry of Figure 9 compared with the prescribed flow depths along the lower mobile wall

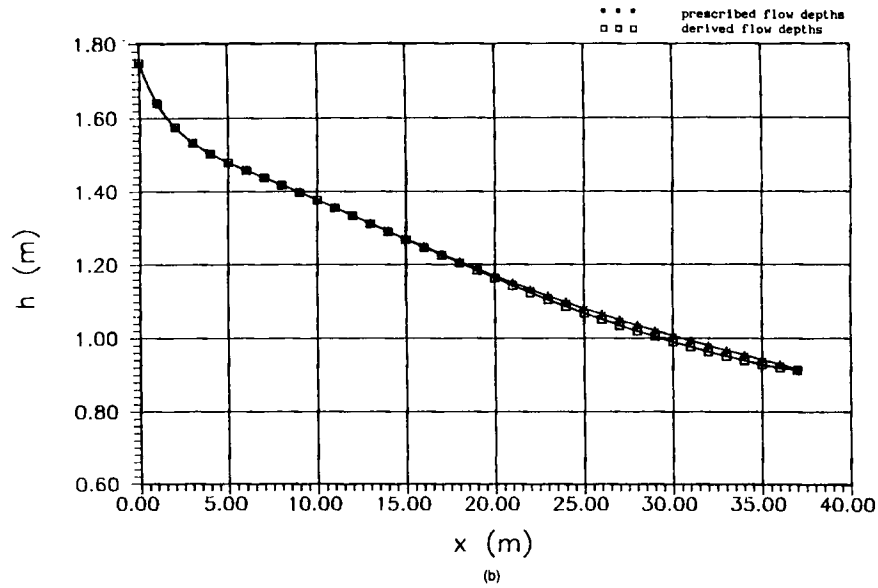

Figure 10(b). The direct solution using the designed geometry of Figure 9 compared with the prescribed flow depths along the upper mobile wall

histories are shown in Figures 4–6. In order to verify that the converged geometry is satisfactory, it was decided to run the analysis code using the designed geometry. These results are shown in Figures 10(a) and 10(b) for the 'lower' and 'upper' side walls respectively. The comparison is considered to be very satisfactory. Slight differences, of the order 1·0%, appear at the 'upper' expansion side wall in the last quarter-region (see Figure 10(b)).

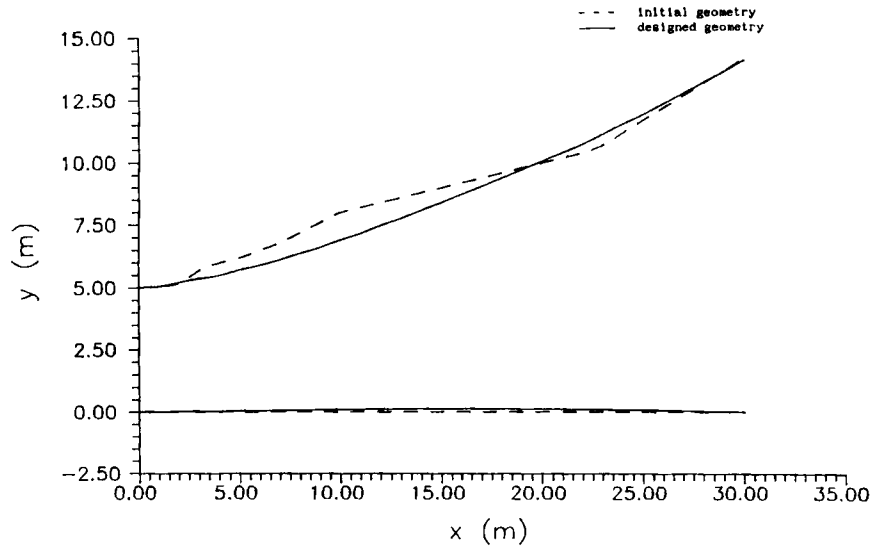

Figure 11. Initial and designed geometries for the Rouse *et al.*[11] expansion design example at $Fr_1 = 2{\cdot}0$

Rouse et al. expansion design at $Fr_1 = 2{\cdot}0$ *(Design* 3)

The gradual channel expansion reported by Rouse *et al.*[11] was used to further evaluate the design ability of the proposed method. The actual channel geometry is given by the formula

$$y/b_1 = \tfrac{1}{2}(x/b_1 2)^{3/2} + \tfrac{1}{2}, \tag{24}$$

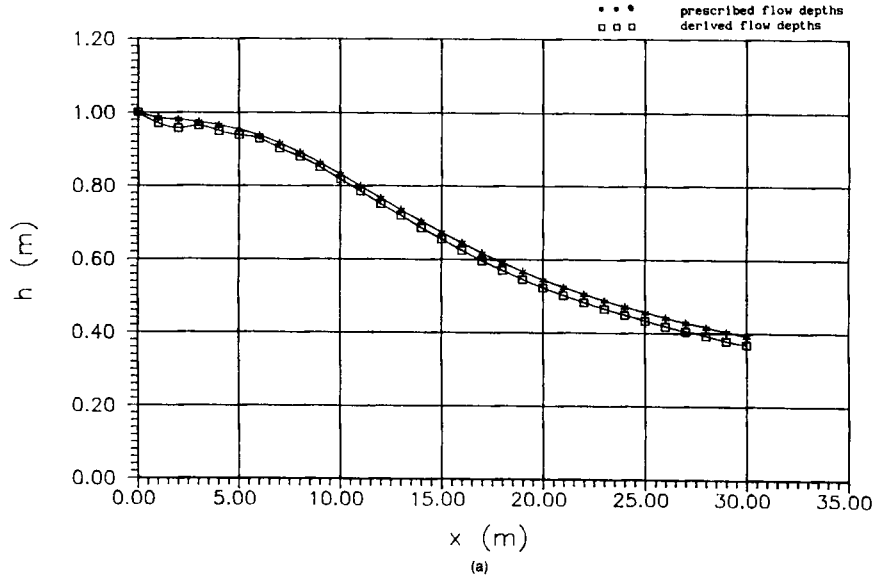

Figure 12(a). The direct solution using the designed geometry of Figure 11 compared with the prescribed flow depths along the lower mobile wall

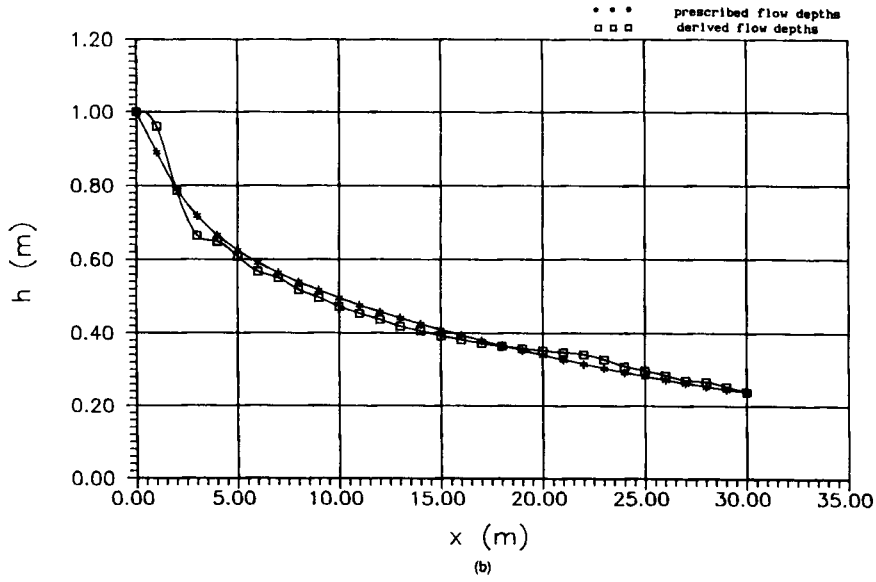

Figure 12(b). The direct solution using the designed geometry of Figure 11 compared with the prescribed flow depths along the upper mobile wall

where b_1 is the channel width at entrance. Figure 11 shows the initial geometry. This geometry was wrongly estimated on purpose. The prescribed flow depths along the 'lower' and 'upper' side walls are shown in Figures 12(a) and 12(b) respectively. These water distributions are the results of the analysis code (see also Reference 16). The resulting (designed) geometry is shown in Figure 11. Once again, in order to verify that the converged geometry is satisfactory, it was decided to run the analysis code using the designed geometry. These results are shown in Figures 12(a) and 12(b). Some differences appear in the first quarter-region of the 'upper' side wall (see Figure 12(b)). The comparison is considered to be satisfactory.

Rouse et al. expansion design at $Fr_1 = 4{\cdot}0$ (Design 4)

When the inlet Froude number is raised to 4·0, a design is sought which will yield the depth distributions of Figures 14(a) and 14(b). The final (designed) geometry is shown in Figure 13. The comparisons between the desired and finally produced depth distributions shown in Figures 14(a) and 14(b) are again satisfactory. Designs 3 and 4 are demanding test cases. To facilitate the convergence procedure the initially set forth geometry of Design 4 was close enough to the expected one (see Figure 13).

Constant depth contraction design (Design 5)

All the previously reported design examples refer to supercritical expansions. The final test case reported herein is a contraction design. In some hydraulic structures it is required that the flow depths be constant and equal to a specific value. In highly inclined supercritical flows, as in the case of steep chutes, the velocity increases in the downstream direction. Flow friction forces do not seriously alter the velocity increase. As a result the flow depth decreases. If constant depths are required, then the geometry must gradually contract. However, this is a delicate problem and a proper solution is sought. Figure 15 shows the initial geometry of a steep chute design required to yield a constant flow depth of 0·6 m. The figure also shows the resulting (designed) geometry.

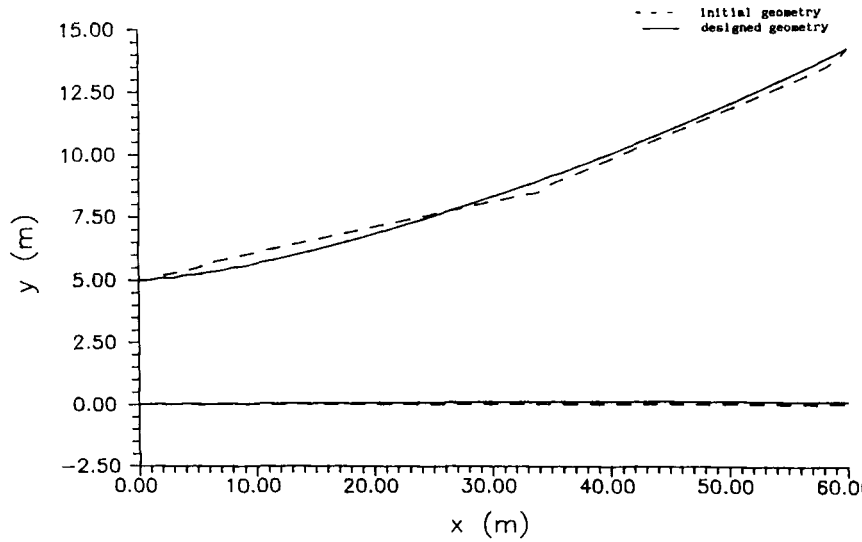

Figure 13. Initial and designed geometries for the Rouse *et al.*[11] expansion design example at $Fr_1 = 4{\cdot}0$

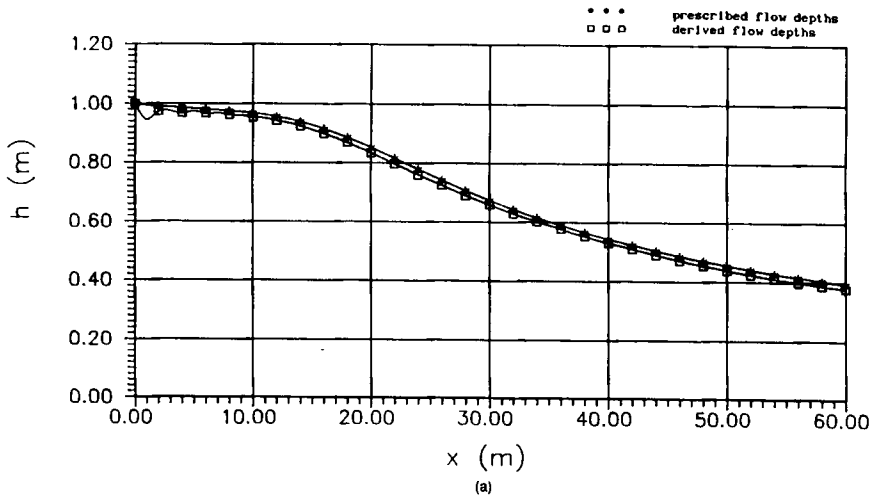

Figure 14(a). The direct solution using the designed geometry of Figure 13 compared with the prescribed flow depths along the lower mobile wall

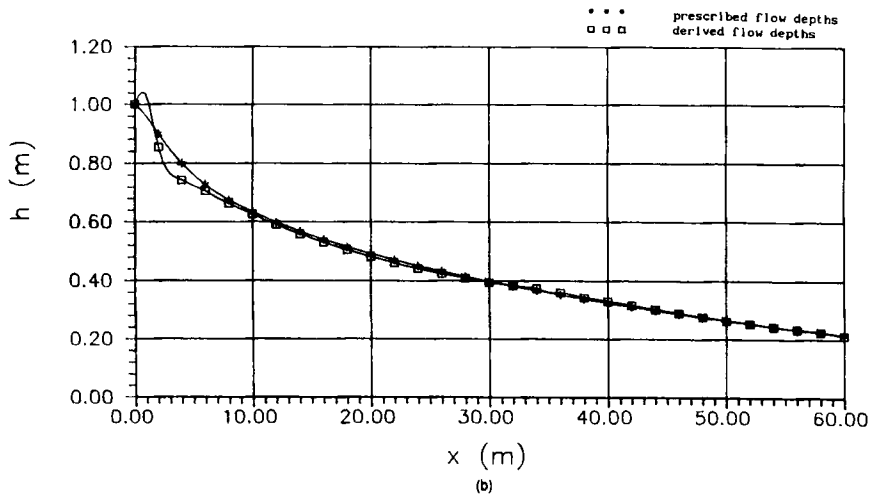

Figure 14(b). The direct solution using the designed geometry of Figure 13 compared with the prescribed flow depths along the upper mobile wall

Figure 16 shows the results of the analysis code using as geometrical data input the designed geometry of Figure15. Again the comparison is equally satisfactory.

CONCLUSIONS

A general numerical method of design has been developed for two-dimensional channel expansions and contractions with prescribed depths along the channel walls. It is a fast and reliable design procedure suitable to run interactively on a minicomputer or a PC. The amount of input data has been kept to a minimum. The marching finite volume analysis code greatly facilitates the

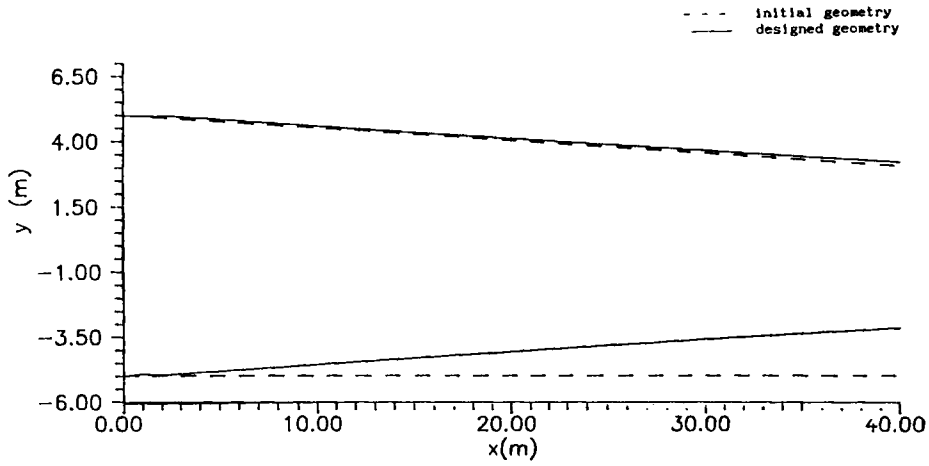

Figure 15. Initial and designed geometries for the constant flow depth design example

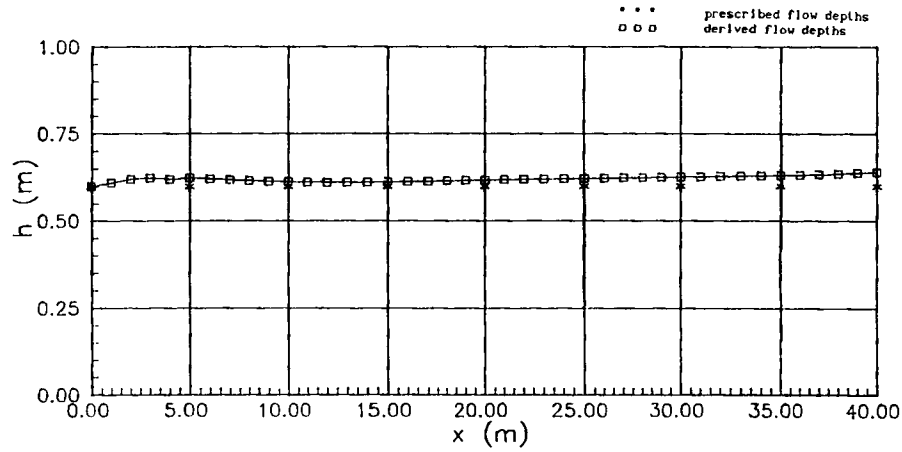

Figure 16. The direct solution using the designed geometry of Figure 15 compared with the prescribed flow depths along the lower mobile wall

straight application of the design procedure. Once the co-ordinates of the new (modified) geometry have been calculated, the formation of the new grid is automatically calculated via the analysis code. The developed method has been applied to generate the geometrical shapes of various channel expansions and contractions operating in supercritical flow. In order to confirm the generated side wall geometry, the co-ordinates of this geometry were used as input data for the analysis code under identical flow conditions. The resulting depth distribution was in very good agreement with the prescribed depth distribution. Numerical experimentation has shown that the amount of CPU time required for design is strictly dependent upon the initial geometry guess. For a typical problem the design procedure needs to be incorporated 20–30 times in order to converge to an acceptable geometry. The method can be used either to generate entire new channel side walls or to modify regions of side wall surfaces.

REFERENCES

1. V. T. Chow, *Open Channel Hydraulics*, McGraw-Hill, New York, 1981, pp. 430–458.
2. F. M. Neilson, 'Convex chutes in converging supercritical flow', *Misc. Paper H-76-19*, Hydraulics Laboratory, U.S. Army Engineer Waterways Experiment Station, 1976.
3. U. K. Singh, 'A design time-marching method for the generation of blades in a cascade', *ASME Paper 86-GT-167*, 1986.
4. T. L. Tranen, 'A rapid computer aided transonic aerofoil design method', *AIAA Paper 74-501*, 1974.
5. J. V. Soulis, 'Thin turbomachinery blade design using a finite-volume method', *Int. j. numer. methods eng.*, **21**, 19–36 (1985).
6. J. D. Stanitz, 'Design of two-dimensional channels with prescribed velocity distributions along the channel walls, I—Relaxation solutions', *NACA TN 2593*, 1952.
7. A. F. Brown and A. Eskandarian, 'Nozzle design using an iterative Dirichlet approach', *Int. j. numer. methods eng.*, **22**, 481–494 (1986).
8. M. Hart and D. S. Whitehead, 'A design method for two-dimensional cascades of turbomachinery blades', *Int. j. numer. methods fluids*, **7**, 1363–1381 (1987).
9. S. S. Tong and W. T. Thomkins Jr., 'A design calculation procedure for shock-free or strong passage shock turbomachinery cascades', *ASME Paper 82-GT-220*, 1982.
10. J. E. Borges, 'A three-dimensional inverse method in turbomachinery, Part I—Theory', *ASME Paper 89-GT-136*, 1989.
11. H. Rouse, B. V. Bhoota and E.-Y. Hsu, 'Design of channel expansions', *Trans. Am. Soc. Civil Eng.*, **116**, 347–363 (1951).
12. A. T. Ippen, 'Mechanics of supercritical flow', *Trans. Am. Soc. Civil Eng.*, **116**, 268–295 (1951).
13. U. Taubert, 'The design of spillway contractions using computer simulation', *Water Power*, (August 1974).
14. R. T. Knapp, 'Design of channel curves for supercritical flow', *Trans. Am. Soc. Civil Eng.*, **116**, 296–325 (1951).
15. W. J. Bauer and E. J. Beck, 'Spillways and stream bed protection works', in C. V. Davis (ed.), *Handbook of Applied Hydraulics*, McGraw-Hill, New York, 1969, Section 20.
16. J. V. Soulis, 'A numerical method for subcritical and supercritical open channel flow calculation', *Int. J. numer. methods fluids*, **13**, 437–464 (1991).
17. J. Hinds, 'The hydraulic design of flume and siphon transitions', *Am. Soc. Civil Eng.*, **92**, 1423–1459 (1928).